ORIGINAL RESEARCH PAPERS

A hybrid radiomics framework integrating genetic algorithm-optimized random forest for preoperative identification of Luminal B breast cancer and Ki-67 prediction: A multicenter study

ZI-MEI LIN[1], YI-JIE CHEN[2], YONG-YUAN XU[1], QING WEN[1], LING-LING CHEN[3], LI-MING SHAO[4], XIAO-YAN NIU[5], LI-NA TANG[2], PIN-TONG HUANG[1]

[1]Department of Ultrasound in Medicine, The Second Affiliated Hospital Zhejiang University School of Medicine, Hangzhou, China; [2]Department of Ultrasound in Medicine, Fujian Cancer Hospital, Fuzhou, China; [3]Department of Ultrasound in Medicine, Cixi Sixth People's Hospital, Cixi, China; [4]Department of Gastroenterology, The Second Affiliated Hospital Zhejiang University School of Medicine, Hangzhou, China; [5]Department of Ultrasound in Medicine, The Affiliated Hospital of Qingdao University, Qingdao, China. Co-first author: Zi-mei Lin, Yi-jie Chen.

ABSTRACT

Background: Preoperative identification of Luminal B breast cancer remains a clinical challenge. This study aimed to develop an ultrasound radiomics framework integrating tumoral and peritumoral information for preoperative identification of Luminal B subtype and prediction of Ki-67 status.

Methods: We retrospectively analyzed 1,944 patients from three centers. The development cohort from Centers One and Two was divided by stratified sampling into a training set (n=1434) and an internal test set (n = 253), and an independent cohort from Center Three was used for external validation. Lesion-containing ROIs were processed using deep learning-assisted segmentation and standardized for downstream analysis. Radiomic features were extracted, and a genetic algorithm (GA) was coupled with a random forest (RF) classifier to construct two models: one for Luminal B classification and another for predicting Ki-67 expression.

Received: 12 February 2026 | Accepted: 31 March 2026

Co-Correspondence: Xiao-yan Niu / The Affiliated Hospital of Qingdao University, Qingdao 262100, China / E-mail: xiaoyan7846@163.com

Li-na Tang / Department of Ultrasound in Medicine, Fujian Cancer Hospital, Fuzhou 350001, China / E-mail: tanglina@fjzlhospital.com

Pin-tong Huang / Department of Ultrasound in Medicine, The Second Affiliated Hospital Zhejiang University School of Medicine, Hangzhou 310009, China; Research Center for Life Science and Human Health, Binjiang Institute of Zhejiang University, Hangzhou, 310053, China / E-mail: huangpintong@zju.edu.cn

Results: The combined tumor-peritumoral model achieved the highest performance, with the Luminal B classifier showing AUCs of 0.876 (training), 0.693 (test), and 0.786 (external validation). The Ki-67 prediction model yielded AUCs of 0.890 (training) and 0.858 (test), though external validation (AUC=0.661) was limited by dataset distribution. The Delong test confirmed that combined ROIs significantly outperformed tumor-only models, with NRI and IDI tests further validating the added value of peritumoral features.
Conclusions: Ultrasound radiomics integrating tumoral and peritumoral regions can support the preoperative identification of Luminal B breast cancer, and peritumoral region analysis significantly enhances predictive performance. The framework also shows potential for predicting Ki-67 status within this subtype.

Key words: Breast Cancer, Radiomics, Ultrasound

Introduction

Breast cancer remains a leading cause of cancer-related mortality in women, with molecular heterogeneity critically influencing prognosis and treatment (1). The luminal B subtype is particularly aggressive, accounting for ~50% of cases. It is characterized by high proliferation, reduced hormone receptor expression, and therapy resistance, conferring a mortality risk over twice that of luminal A tumors (2-4). Subtypes include HER2-negative (B1, Ki-67>14%) and HER2-positive (B2) categories, each with distinct outcomes (5-8). Current diagnosis relies on invasive, costly IHC or genomic assays, while conventional imaging lacks specificity for luminal subtyping. Emerging evidence suggests peritumoral features (e.g., vascularity, immune infiltration) may hold key biological information, yet they remain underexplored (9,10).

Artificial intelligence offers promising solutions. Machine and deep learning models show potential in improving breast cancer classification by integrating multimodal data (11,12). Ultrasound radiomics features have demonstrated preliminary correlations with receptor status, but existing models often lack specificity for luminal B (13-15). This study aimed to investigate distinct imaging phenotypes of luminal B tumors by integrating intratumoral and peritumoral radiomic features from ultrasound. We developed a machine learning model, utilizing deep learning for automated ROI segmentation to noninvasively perform molecular subtyping. Our focus was on differentiating luminal B and predicting Ki67 expression within this subtype, to facilitate earlier, more precise therapeutic decisions.

Methods and Materials

Patients

The training and internal testing sets in this retrospective study were collected from Center One and Center Two from January 2017 to December 2024, while the external testing set was collected from Center Three from January 2016 to December 2024. This study was approved by the institutional ethics committees of all hospitals (NO. Y20230427, QYFYWZLL30450, K2023-421-01), and the requirement for informed consent from the patients was waived by the institutional review boards of The Second Affiliated Hospital Zhejiang University School of Medicine, The Affiliated Hospital of Qingdao University, and Fujian Cancer Hospital. The inclusion criteria: breast cancer patients with complete pathology, no preoperative therapy, surgery within 30 days after ultrasound, and complete clinical data. The exclusion criteria: nonmass lesions without delineated boundaries, biopsy before ultrasound, previous metastasis/other malignancies, and poor image quality.

Data collection and preprocessing

Given the retrospective, multicenter design of this study, imaging data were acquired as part of routine

clinical practice across participating institutions. Consequently, acquisition protocols—including scanner models, probe types, and imaging settings—were site-specific and not centrally controlled, reflecting real-world clinical heterogeneity. To mitigate potential variability introduced by differences in acquisition protocols, all images underwent a standardized preprocessing pipeline prior to feature extraction, as described below. Detailed equipment parameters for all centers are summarized as follows. The breast US images of all patients were acquired using US manufactured by Mindary (L14-3WU, R7S, R9; Guangzhou, China), Canon (i18LX5, i900; Tokyo, Japan), Esaote (LA523, MyLab 90; Genoa, Italy), GE Logiq E9 (ML6-15, GE Healthcare, Milwaukee, WI, USA), Philips (L12-5, EPIQ; Eindhoven, Holland), or SuperSonic (SL15-4, Aixplorermach30; SuperSonic Imagine, France). The US images were evaluated by two breast radiologists (with 7 and 12 years of experience interpreting breast US images) who were blinded to the clinical information but not to the age of each patient. In cases of disagreement, the radiologists discussed the issue and reached a consensus.

Clinical, pathological, and follow-up data were collected via electronic records. Molecular subtypes were classified based on receptor expression, with luminal B further stratified by Ki-67 index (cutoff 14%). Histopathological examination served as the gold standard. The histological grade and expression of the estrogen receptor (ER), progesterone receptor (PR), human epidermal growth factor receptor 2 (HER2), and cell proliferation-associated Ki67 antigens were determined by immunohistochemical analysis.

Model construction

Finally, a total of 1944 women (mean age = 51 years; range =23–86 years) were included in this retrospective study (5321 images), including 917 patients in the luminal B subgroup and 1027 patients in the non–luminal B subgroup (Table 1). All patients from Centers One and Two were randomly divided into a training set with 1434 patients and an internal testing set with 253 patients, with a ratio of 8.5:1.5. A total of 257 patients from Center Three were included in the external testing set (Figure 1).

Table 1. Basic characteristics of participants.

Characteristic Statistic	Pathology		*P*
	Luminal B	Non-Luminal B	
Number	917	1027	—
Age (y)	54.40 ± 11.22 (23.00–86.00)	54.37 ± 11.61 (23.00–87.00)	0.95
Lesion size (cm)	2.15 ± 1.33 (0.10–18.00)	2.28 ± 1.96 (0.20–20.00)	0.08

Image preprocessing included lesion localization using radiologist-guided ROI annotation and mask information, followed by standardization of model inputs to 256 × 256 pixels for downstream processing (Figure 2).

Tumor segmentation employed a U-Net++ architecture with a ResNet50 encoder initialized with ImageNet pretrained weights. Pixelwise classification was achieved through sigmoid activation outputs. During training, data augmentation, Dice-based optimization, Adam optimization, and cosine-annealing scheduling were applied to improve robustness. In the overall workflow, the segmentation module served as an assistive preprocessing step rather than the primary methodological contribution of the study.

Peritumoral regions were defined as those with 2 mm concentric expansions beyond the tumor boundaries, excluding areas that overlapped the pectoral muscles or adipose tissue, as confirmed by threshold-based masking. We now explicitly acknowledge that radiologist-guided lesion localization reduces the difficulty of the downstream segmentation task and should be considered when interpreting this component of the pipeline.

Radiomic feature extraction

Quantitative features were extracted from both intratumoral and peritumoral ROIs across four domains:

- Morphological: Circularity, aspect ratio, and Hu moment invariants (orders 1–7).
- Textural: Contrast, homogeneity, correlation, and entropy derived from the gray-level co-occurrence matrix (GLCM).
- Intensity-based: First-order statistics including mean intensity, standard deviation, skewness, kurtosis, and energy.

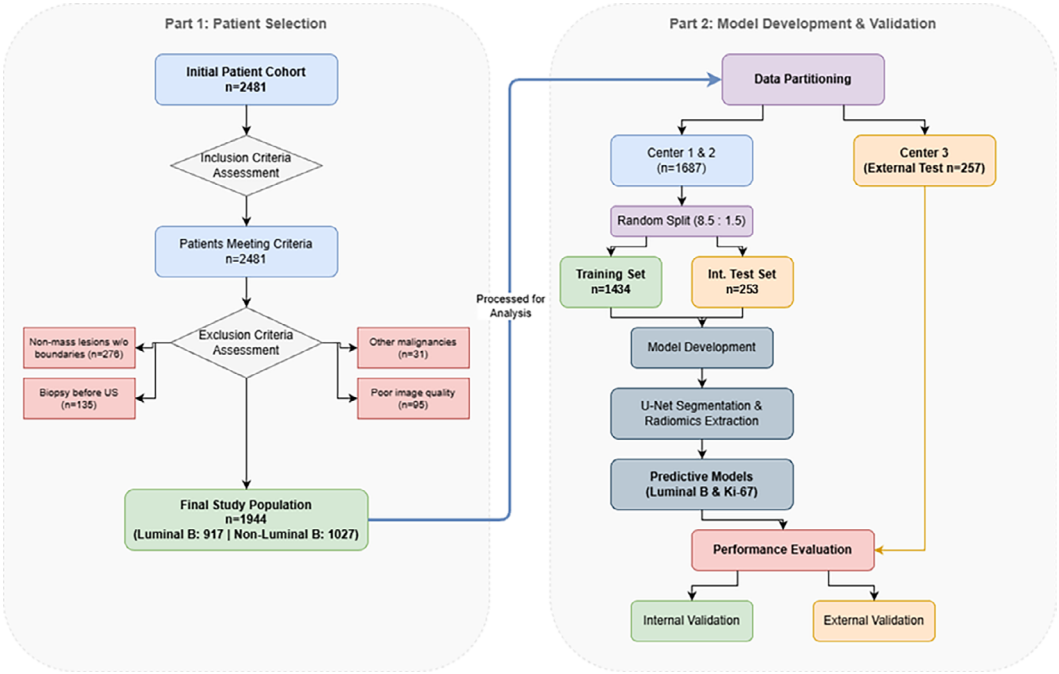

Figure 1. Flowchart.

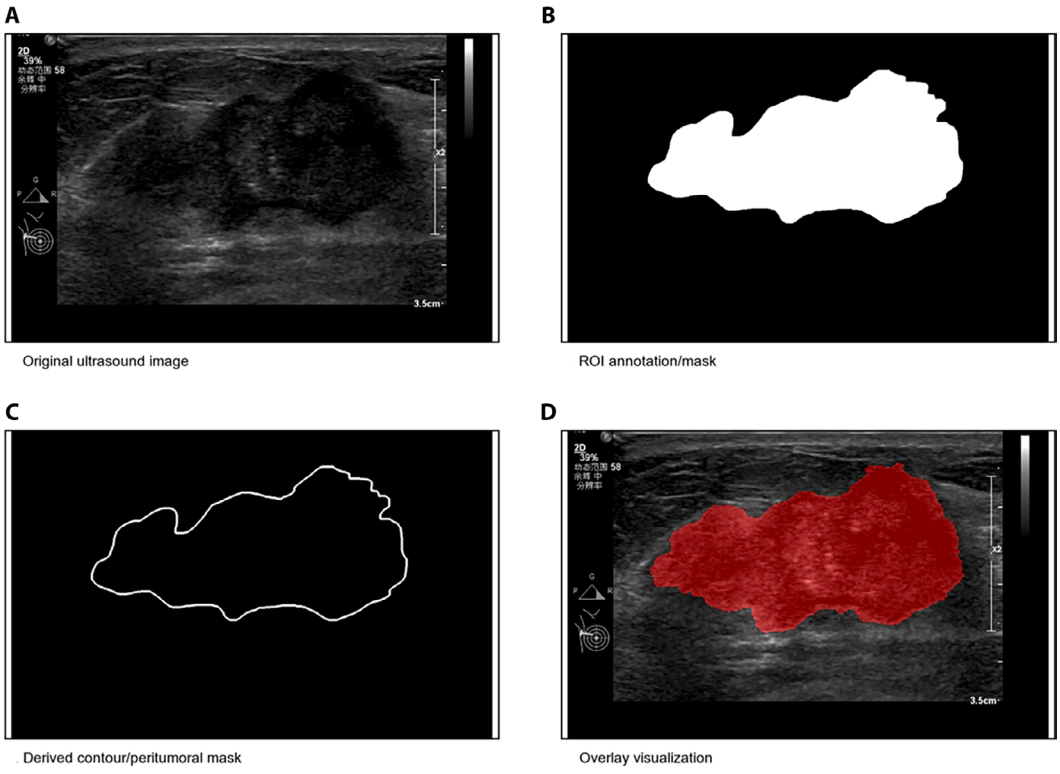

Figure 2. Representative example of the image-processing workflow. (A) Original ultrasound image. (B) ROI annotation/mask. (C) Derived contour/peritumoral mask. (D) Overlay visualization for visual inspection.

Calcification metrics: Microcalcification count and total calcified area.

Peritumoral-specific: Sharpness count, mean intensity gradient magnitude (margin analysis), radial spicule count, and complexity index (branching ratio).

In total, 43 candidate variables, including handcrafted image-derived features and the clinical variable age, were entered into the modeling pipeline.

Model construction and optimization

Hybrid Feature Selection and Classification Framework

We implemented a hybrid framework integrating a genetic algorithm (GA) for feature selection with a random forest (RF) classifier. The GA encoded feature subsets using binary vectors corresponding to the input features and utilized uniform crossover (probability=0.9) and bit-flip mutation. Initial populations were seeded with predefined combinations to accelerate convergence. The fitness function was designed to maximize recall (Fitness = -Recall) to prioritize the sensitivity for identifying the aggressive Luminal B subtype.

Random forest optimization

The RF hyperparameters were automatically tuned to maximize recall for the target subtype (Luminal B). The search space included:

Number of trees: 100–1500
Maximum depth: 5–20
Minimum samples for split/leaf: 2–20
Feature selection strategy: {$\sqrt{p}$, $\log_2$ (features), all features}

Bootstrap sampling enabled

GA Fitness Evaluation and Termination Candidate solutions were evaluated by training an RF model on the selected feature subset and calculating its recall. The fitness function was defined as Fitness = -Recall. Solutions with fewer than 3 selected features were excluded as a heuristic stability constraint to avoid degenerate and highly unstable feature subsets. The optimization terminated after 10 generations or if the fitness improvement was below 1e-3 for 10 consecutive generations.

Validation and Interpretability

Data were split using stratified sampling (85% training, 15% testing) to preserve class distribution. To address the inherent class imbalance between Luminal B and non-Luminal B subtypes, the Synthetic Minority Over-sampling Technique (SMOTE) was applied to the training data. Features were standardized (Z-score normalization) prior to model input. Model interpretability was enhanced by analyzing a core feature subset identified through recursive elimination, focusing on high-frequency features such as morphological descriptors, texture metrics, Hu moments, and clinical variables like age. Hyperparameter optimization employed 5-fold cross-validation, and the final model was evaluated on the hold-out test set and external validation cohort.

Statistical analysis

Feature reliability was assessed via intraclass correlation coefficient (ICC>0.75 retained). To address the class imbalance, the Synthetic Minority Over-sampling Technique (SMOTE) was applied to the training data. (16). Nonparametric tests (Wilcoxon rank-sum) and receiver operating characteristic (ROC) analysis were performed. Model performance was evaluated using the area under the ROC curve (AUC), sensitivity, specificity, positive predictive value (PPV), negative predictive value (NPV), and accuracy ($p<0.05$ significant, FDR correction).The DeLong test was employed to statistically compare the AUCs between models (e.g., tumor-only vs. combined regions). Feature selection was conducted using the Genetic Algorithm (GA) as described in the methodology. Seven additional classifiers were compared (decision tree (DT), k-nearest neighbors (KNN), support vector machine (SVM), Bayesian classifiers, kernel approximation classifiers, ensemble classifiers, and neural network classifiers). Analyses were conducted in Python (Pytorch framework) and MATLAB R2023b.

Results

A total of 43 candidate variables were entered into the modeling pipeline, including morphological characteristics (e.g., circularity and aspect ratio), seven Hu moment invariants, textural features (contrast, homogeneity, and their extreme values), gray-level histogram statistics (entropy, skewness, kurtosis, among others), margin- and calcification-related attributes, and the clinical variable age. The target variable was the molecular subtype, classified as either luminal B or non-luminal B. Stratified sampling was employed for partitioning, and oversampling techniques were applied to the training set to mitigate class imbalance (Figures 3-5). Feature reduction was then performed using the genetic algorithm-based subset-selection procedure before random forest modeling.

Model performance

Luminal B classification model

Recall was established as the primary evaluation metric to prioritize the sensitivity for identifying the aggressive Luminal B subtype. The genetic algorithm-optimized Random Forest (GA-RF) model demonstrated robust performance on the independent test set, achieving a recall (sensitivity) of 81%. Specifically, the model correctly identified 124 out of 154 Luminal B cases (False Negative Rate: 19.5%), minimizing the risk of missed diagnoses in a clinical setting. Regarding specificity, 81 out of 138 non-Luminal B cases were correctly classified (False Positive Rate: 41.3%). The classification report indicated a precision of 70% for Luminal B, with both overall accuracy and the macro F1-score reaching 70% (Figure 6).

Hyperparameter optimization by using Optuna identified the optimal model configuration (1,622 trees, max depth of 44, max_features='sqrt'), which yielded a consistent recall of 72.97% during 5-fold cross-validation, confirming the model's stability prior to testing.

Ki-67 Expression Prediction Model

For the prediction of Ki-67 expression status (High vs. Low) within the Luminal B cohort, the model exhibited excellent generalization capability with minimal overfitting. The AUC values were 0.890 in the training set and 0.858 in the internal testing set, reflecting a high degree of consistency. In the external validation cohort, the model achieved an AUC of 0.661. The corresponding prediction accuracies were 97.18% (training), 85.51% (internal test), and 97.67% (external validation). The high accuracy in the external set, despite a moderate AUC, likely reflects the class imbalance within the cohort (Table 2).

Discussion

Breast cancer is a molecularly and clinically heterogeneous disease. The luminal B subtype is particularly aggressive, marked by high proliferation, therapy resistance, and poor prognosis, and is linked to higher local recurrence and bone metastasis rates than non-inflammatory breast cancers (17). Its preoperative identification remains a major clinical challenge. In this multicenter study, we developed a deep learning radiomics model using ultrasound to noninvasively predict luminal B status. The integrated model, combining tumor and peritumoral features, outperformed tumor-only approaches, underscoring the tumor microenvironment's importance and offering a promising tool for preoperative molecular subtyping.

The enhanced performance of the combined model—supported by a significantly increased AUC in the test set and confirmed by the Delong test—aligns with growing evidence that the peritumoral region harbors critical biological information related to tumor aggression and metastatic potential (18-20). Radiomic features reflecting desmoplastic reaction, inflammatory infiltration, and angiogenesis likely underlie this improvement. Furthermore, NRI and IDI analyses confirmed that the inclusion of peritumoral features significantly improved the classification ability.

Luminal B breast cancer is clinically distinct: Studies indicate that over time, some patients may develop features resembling those of triple-negative or HER2-positive disease (21,22), whereas luminal A tumors have a comparatively favorable prognosis. Luminal B cancers typically display higher histological grades and reduced responsiveness to endocrine

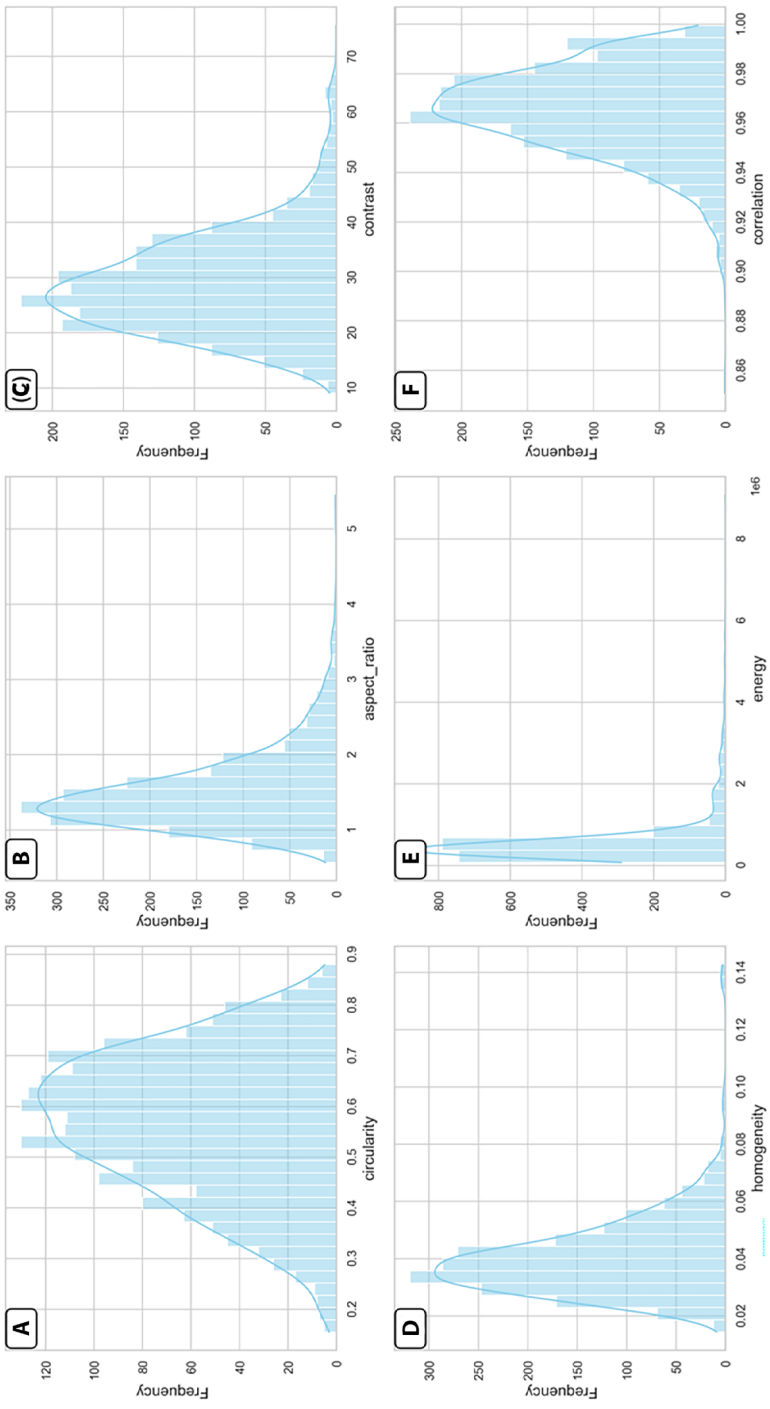

Figure 3. Frequency distribution histogram. Each subgraph displays the distribution of a specific feature (A. circularity, B. aspect_ratio, C. contrast, D. homogeneity, E. energy, F. correlation)

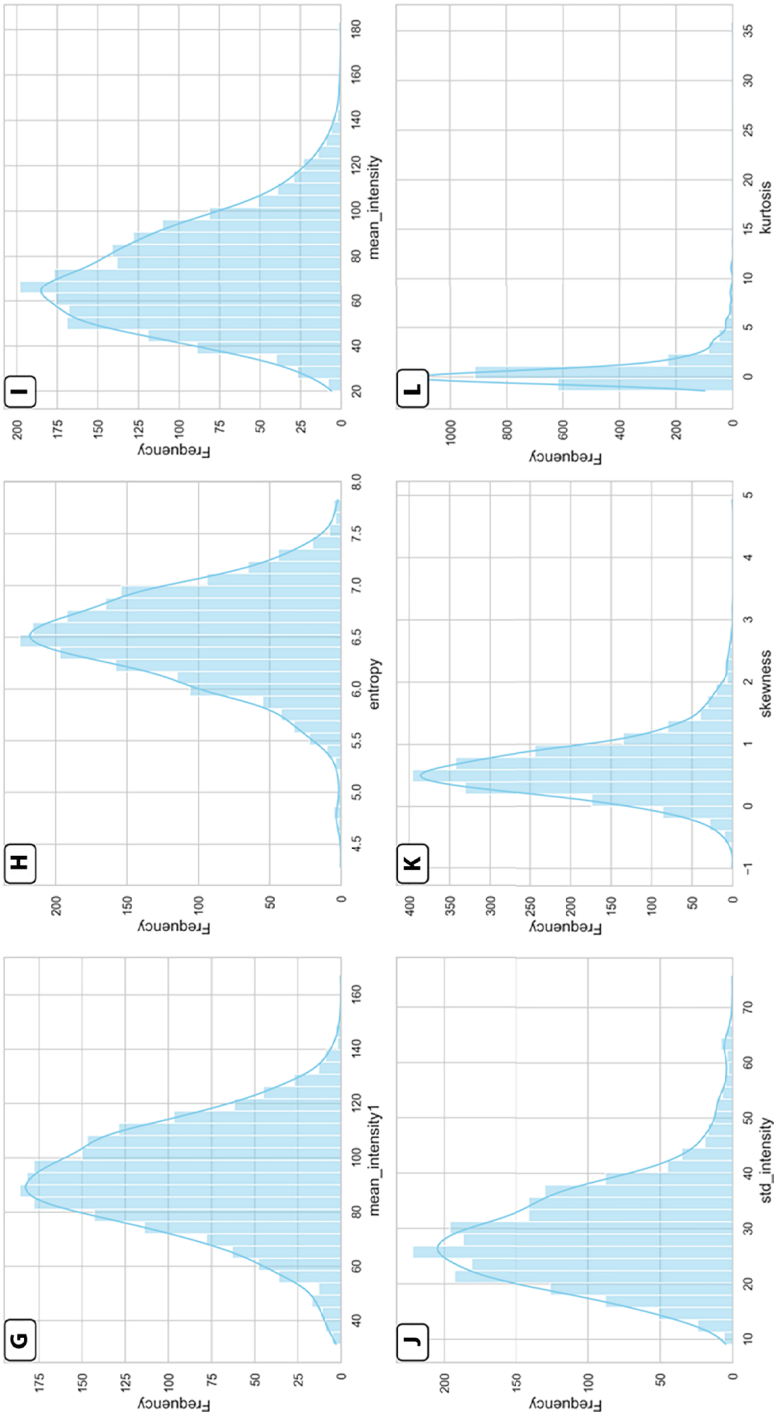

Figure 4. Frequency distribution histogram. Each subgraph displays the distribution of a specific feature (G. mean_intensity1, H. entropy, I. mean_intensity, J. std_intensity, K. skewness, L. kurtosis.

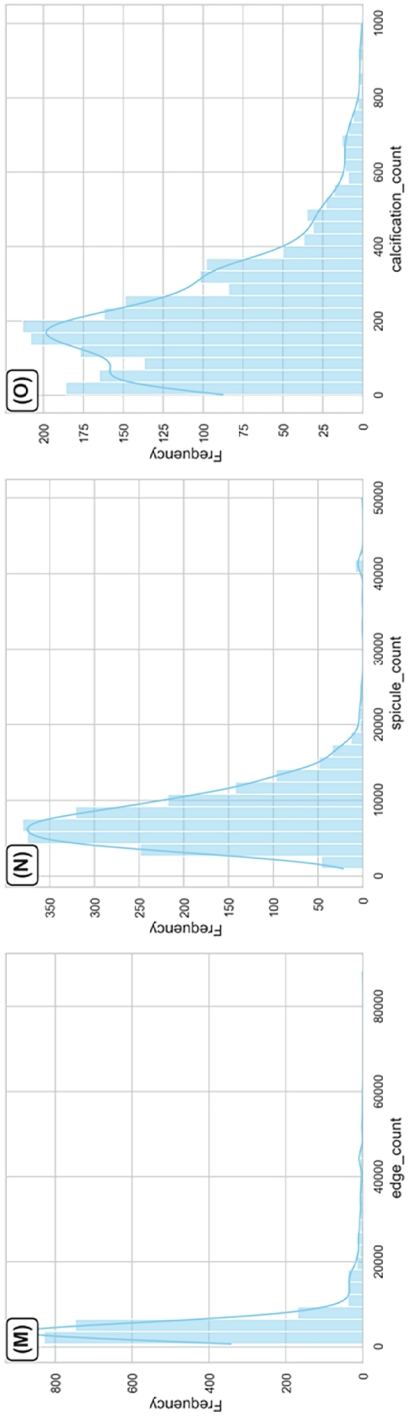

Figure 5. Frequency distribution histogram. Each subgraph displays the distribution of a specific feature (M. edge_count, N. spicule_count, O. calcification_count).

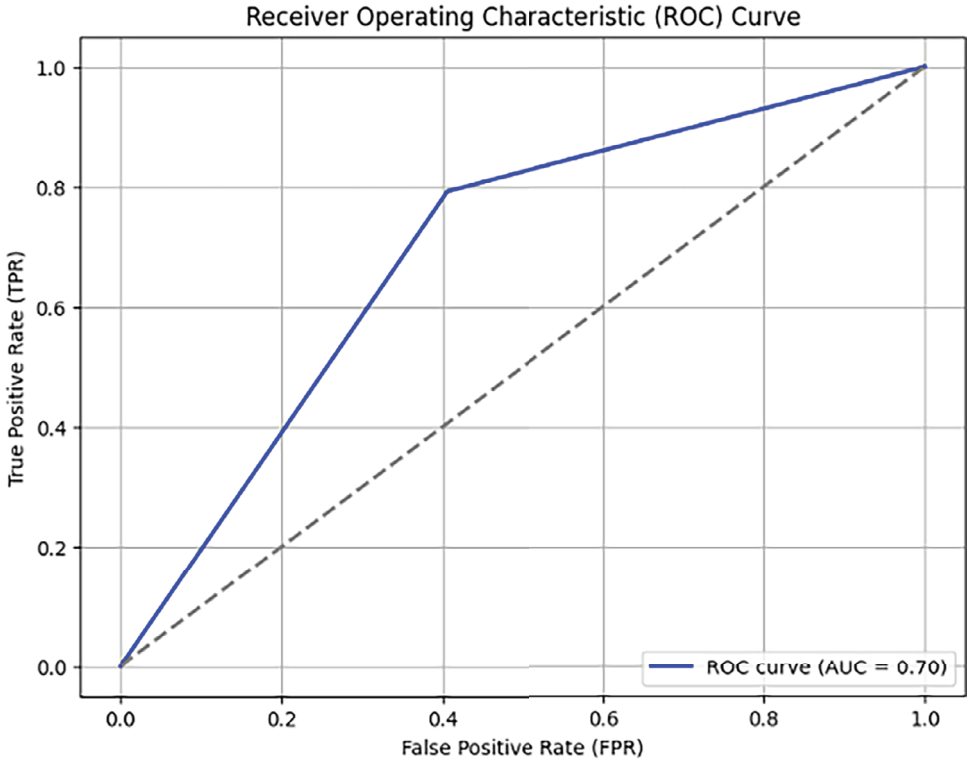

Figure 6. ROC curve of the model.

therapy (23). Moreover, the luminal B subgroup is heterogeneous; for instance, the HER2-low, PR-low, and Ki-67-high subgroups may constitute distinct entities (2). Our model achieved a recall of 81% for luminal B identification, demonstrating high sensitivity, which isa critical attribute for minimizing missed diagnoses. The precision of 70% and overall accuracy of 70% reflect balanced performance despite the class imbalance. However, the 19.5% false-negative rate (30/154 missed cases) warrants further improvement to reduce potential delays in treatment.

Methodologically, the combination of genetic algorithm (GA) feature selection and random forest (RF) classification effectively handled high-dimensional radiomic data. The selected features included morphological (e.g., sphericity and aspect ratio), textural (e.g., contrast and entropy), and Hu moment invariants, indicating distinct geometric and textural patterns in luminal B tumors. Age also contributed significantly to classification, possibly reflecting age-related tumor biological differences. Hyperparameter optimization via Optuna yielded a robust model (recall: 72.97% in validation, 81% in testing), affirming the efficacy of the GA-RF pipeline.

Although stratified sampling and oversampling were used to address class imbalance (luminal B vs. non–luminal B≈2.45:1), the false-positive rate of 41.3% (57/138 non-luminal B misclassified) indicates limited specificity. Overlapping radiomic phenotypes across subtypes or insufficient feature resolution may account for this. Techniques such as synthetic minority oversampling or cost-sensitive learning may improve specificity in future studies.

The luminal B classification model demonstrated generalizability, with AUCs of 0.693 (test set) and 0.786 (external validation) supporting its applicability across diverse cohorts and imaging protocols. In contrast, the Ki-67 prediction model performed well on the internal data (AUC: 0.890 training, 0.858 test) but poorly on the external validation data (AUC: 0.661), likely because of dataset shifting and an imbalanced Ki-67 distribution. These results underscore the need

Table 2. Diagnostic efficiency of each model

Model Type	Dataset	AUC (95% CI)	Accuracy	Sensitivity (Recall)	Specificity	PPV	NPV	F1-Score
Luminal B Classification								
Tumor-Only Model	Training	0.765 (0.742–0.788)	0.712	0.684	0.735	0.688	0.731	0.686
	Internal Test	0.612 (0.554–0.670)	0.623	0.584	0.667	0.664	0.588	0.621
	External Val	0.701 (0.645–0.757)	0.658	0.642	0.674	0.663	0.653	0.652
Combined Model (Tumor+Peritumoral)	Training	0.876 (0.858–0.894)	0.814	0.835	0.796	0.782	0.847	0.808
	Internal Test	0.693 (0.635–0.751)	0.7	0.81	0.587	0.7	0.717	0.7
	External Val	0.786 (0.732–0.840)	0.743	0.792	0.695	0.722	0.768	0.755
Ki-67 Prediction								
Combined Model	Training	0.890 (0.871–0.909)	0.972	0.965	0.982	0.988	0.947	0.976
	Internal Test	0.858 (0.812–0.904)	0.855	0.884	0.785	0.903	0.746	0.893
	External Val	0.661 (0.589–0.733)	0.977	0.99	0.208	0.985	0.294	0.987

for external validation on representative cohorts to ensure model robustness. Clinically, our model may serve as a valuable preoperative tool for early risk stratification, helping clinicians identify patients who may require more aggressive treatment. It should be regarded as a complement to, not a replacement for, standard immunohistochemical profiling.

Although our model's recall (81%) and precision (73% in validation) exceed those of many previous radiomics studies, likely owing to peritumoral feature inclusion and rigorous feature selection, several limitations remain. First, the 30% false-positive rate may lead to unnecessary biopsies. Second, although informative, radiomic features such as Hu moments lack clear biological interpretation. Third, despite the multicenter design, variability in imaging protocols may still affect feature stability. Future work should incorporate genomic or histopathological data, refine peritumoral characterization using advanced spatial analyses, and emphasize prospective validation in real-world settings. In addition, a formal ablation study of preprocessing and model components was not performed in the present work, and this should be addressed in future studies.

In conclusion, this study highlights the value of peritumoral radiomic analysis based on ultrasound imaging for the preoperative identification of luminal B breast cancer. Future efforts should focus on prospective validation, multimodal data integration, and the mechanistic interpretation of radiomic features to increase clinical utility.

Acknowledgements: The authors wish to express their sincere gratitude to Mr Haoran Zhao for his expert guidance on the statistical analysis of this study.

Authors Contributions: Zimei Lin: Writing – original draft, Visualization, Validation, Soft- ware, Methodology, Investigation, Formal analysis, Data curation, Conceptualization. Yijie Chen: Writing – review & editing, Writing – original draft, Visualization, Validation, Methodology, Investigation, Formal analysis, Data curation. Yongyuan Xu: Writing – review & editing, Validation, Resources, Data curation, Conceptualization. Qing Wen: Writing – review & editing, Visualization, Supervision, Soft- ware, Resources, Project administration, Methodology, Investigation, Data curation, Conceptualization. Lingling Chen: Writing – review & editing, Visualization, Resources, Project administration, Methodology, Investigation, Data curation, Funding acquisition, Conceptualization. Liming Shao: Writing – review & editing, Visualization, Resources, Project administration, Methodology, Investigation, Funding

acquisition, Conceptualization. Xiaoyan Niu: Writing – review & editing, Visualization, Resources, Project administration, Methodology, Investigation, Data curation, Conceptualization. Lina Tang: Writing – review & editing, Visualization, Resources, Project administration, Methodology, Investigation, Conceptualization. Pintong Huang: Writing – review & editing, Supervision, Methodology, Investigation, Funding acquisition, Conceptualization.

Funding: This study has received funding by Liming Shao (The Zhejiang Provincial Natural Science Foundation of China, TGD23H160009), Lingling Chen (The Cixi Municipal Science and Technology Plan Project, CN2023020)), and Pintong Huang (The National Natural Science Foundation of China (82030048, 82230069).

Ethics Approval: T Institutional Review Board approval was obtained.

Conflict of Interest: The authors of this manuscript declare no relationships with any companies, whose products or services may be related to the subject matter of the article.

Statistics and Biometry: Statistical analysis and model construction were performed using Python (Pytorch) and MATLAB R2023b. The analysis included complex statistical methods such as Genetic Algorithms (GA) for feature selection, Random Forest (RF) classification, U-Net++ for deep learning segmentation, and the DeLong test for comparing ROC curves.

Informed Consent: Written informed consent was waived by the Institutional Review Board.

Methodology. Methodology: retrospective diagnostic or prognostic study; multicenter study

Declaration on the Use of AI: AI was used only for grammar correction. All AI-suggested changes were reviewed and approved by a human author and by AJE.

References

1. Perou CM, Sørlie T, Eisen MB, van de Rijn M, Jeffrey SS, Rees CA, et al. Molecular portraits of human breast tumours. Nature. 2000;406(6797):747-52. doi: 10.1038/35021093.
2. Cheang MC, Chia SK, Voduc D, Gao D, Leung S, Snider J, et al. Ki67 index, HER2 status, and prognosis of patients with luminal B breast cancer. J Natl Cancer Inst. 2009;101(10):736-50. doi: 10.1093/jnci/djp082.
3. Ades F, Zardavas D, Bozovic-Spasojevic I, Pugliano L, Fumagalli D, de Azambuja E, et al. Luminal B breast cancer: molecular characterization, clinical management, and future perspectives. J Clin Oncol. 2014;32(25):2794-803. doi: 10.1200/JCO.2013.54.1870.
4. Loo SK, Yates ME, Yang S, Oesterreich S, Lee AV, Wang XS. Fusion-associated carcinomas of the breast: Diagnostic, prognostic, and therapeutic significance. Genes Chromosomes Cancer. 2022;61(5):261-73. doi: 10.1002/gcc.23020.
5. Li Y, Du W, Yang R, Wei X, Li H, Zhang X. Copper Chaperone for Superoxide Dismutase Subtypes as a Prognostic Marker in Luminal B Breast Cancer. Clin Med Insights Oncol. 2024;18:11795549231219239. doi: 10.1177/11795549231219239.
6. Samiei S, Simons JM, Engelen SME, Beets-Tan RGH, Classe JM, Smidt ML. Axillary Pathologic Complete Response After Neoadjuvant Systemic Therapy by Breast Cancer Subtype in Patients With Initially Clinically Node-Positive Disease: A Systematic Review and Meta-analysis. JAMA Surg. 2021;156(6):e210891. doi: 10.1001/jamasurg.2021.0891.
7. Meyer-Wilmes P, Huober J, Untch M, Blohmer JU, Janni W, Denkert C, et al. Long-term outcomes of a randomized, open-label, phase II study comparing cabazitaxel versus paclitaxel as neoadjuvant treatment in patients with triple-negative or luminal B/HER2-negative breast cancer (GENEVIEVE).ESMOOpen.2024;9(5):103009.doi:10.1016/j.esmoop.2024.103009.
8. Camargo-Herrera V, Castellanos G, Rangel N, Jiménez-Tobón GA, Martínez-Agüero M, Rondón-Lagos M. Patterns of Chromosomal Instability and Clonal Heterogeneity in Luminal B Breast Cancer: A Pilot Study. Int J Mol Sci. 2024;25(8):4478. doi: 10.3390/ijms25084478.
9. Badwe RA, Parmar V, Nair N, Joshi S, Hawaldar R, Pawar S, et al. Effect of Peritumoral Infiltration of Local Anesthetic Before Surgery on Survival in Early Breast Cancer. J Clin Oncol. 2023;41(18):3318-28. doi: 10.1200/JCO.22.01966.
10. Jiang L, You C, Xiao Y, Wang H, Su GH, Xia BQ, et al. Radiogenomic analysis reveals tumor heterogeneity of triple-negative breast cancer. Cell Rep Med. 2022;3(7):100694. doi: 10.1016/j.xcrm.2022.100694.
11. Zhang J, Wu J, Zhou XS, Shi F, Shen D. Recent advancements in artificial intelligence for breast cancer: Image augmentation, segmentation, diagnosis, and prognosis approaches. Semin Cancer Biol. 2023;96:11-25. doi: 10.1016/j.semcancer.2023.09.001.
12. Kurozumi S, Ball GR. Research on biomarkers using innovative artificial intelligence systems in breast cancer. Int J Clin Oncol. 2024;29(11):1669-75. doi: 10.1007/s10147-024-02602-3.

13. Qi YJ, Su GH, You C, Zhang X, Xiao Y, Jiang YZ, et al. Radiomics in breast cancer: Current advances and future directions. Cell Rep Med. 2024;5(9):101719. doi: 10.1016/j.xcrm.2024.101719.
14. Conti A, Duggento A, Indovina I, Guerrisi M, Toschi N. Radiomics in breast cancer classification and prediction. Semin Cancer Biol. 2021;72:238-50. doi: 10.1016/j.semcancer.2020.04.002.
15. Davey MG, Davey MS, Boland MR, Ryan ÉJ, Lowery AJ, Kerin MJ. Radiomic differentiation of breast cancer molecular subtypes using pre-operative breast imaging - A systematic review and meta-analysis. Eur J Radiol. 2021;144:109996. doi: 10.1016/j.ejrad.2021.109996.
16. Gu X, Angelov PP, Soares EA. A Self-Adaptive Synthetic Over-Sampling Technique for Imbalanced Classification. Int J Intell Syst. 2020;35:923-43. doi: 10.1002/int.22245.
17. Malik JA, Ahmed S, Jan B, Bender O, Al Hagbani T, Alqarni A, et al. Drugs repurposed: An advanced step towards the treatment of breast cancer and associated challenges. Biomed Pharmacother. 2022;145:112375. doi: 10.1016/j.biopha.2021.112375.
18. Lin P, Xie W, Li Y, Zhang C, Wu H, Wan H, et al. Intratumoral and peritumoral radiomics of MRIs predicts pathologic complete response to neoadjuvant chemoimmunotherapy in patients with head and neck squamous cell carcinoma. J Immunother Cancer. 2024;12(11):e009616. doi: 10.1136/jitc-2024-009616.
19. Yao J, Jia X, Zhou W, Zhu Y, Chen X, Zhan W, et al. Predicting axillary response to neoadjuvant chemotherapy using peritumoral and intratumoral ultrasound radiomics in breast cancer subtypes. iScience. 2024;27(9):110716. doi: 10.1016/j.isci.2024.110716.
20. Luo S, Chen X, Yao M, et al. Intratumoral and peritumoral ultrasound-based radiomics for preoperative prediction of HER2-low breast cancer: a multicenter retrospective study. Insights Imaging. 2025;16(1):53. doi: 10.1186/s13244-025-01934-6.
21. Luo S, Chen X, Yao M, Ying Y, Huang Z, Zhou X, et al. High Expression of PKCζ And CTNNBIP1 Is Associated With Poor Prognosis in Luminal B Breast Cancer. Cancer Genomics Proteomics. 2025;22(4):538-56. doi: 10.21873/cgp.20520.
22. Zagami P, Fernandez-Martinez A, Rashid NU, Hoadley KA, Spears PA, Curigliano G, et al. Association of PIK3CA Mutation With Pathologic Complete Response and Outcome by Hormone Receptor Status and Intrinsic Subtype in Early-Stage ERBB2/HER2-Positive Breast Cancer. JAMA Netw Open. 2023;6(12):e2348814. doi: 10.1001/jamanetworkopen.2023.48814.
23. Du X, Zhou Z, Shao Y, Qian K, Wu Y, Zhang J, et al. Immunoarchitectural patterns as potential prognostic factors for invasive ductal breast cancer. NPJ Breast Cancer. 2022;8(1):26. doi: 10.1038/s41523-022-00389-y.

Copyright: The Author(s), 2026. Licensee Mattioli 1885, Fidenza, Italy. This is an open-access article distributed under the terms of the Creative Commons Attribution NonCommercial License (CC BY-NC-4.0).

Disclaimer/Publisher's Note: The statements, opinions and data contained in this article are solely those of the author(s) and contributor(s) and do not necessarily reflect those of their affiliated organizations, the publisher, the editors or the reviewers. The publisher and the editors disclaim any responsibility for injury to people or property resulting from any ideas, methods, instructions or products mentioned in the content. Any product that may be evaluated in this article, or claim made by its manufacturer, is not guaranteed or endorsed by the publisher.